International Journal of Biological Macromolecules 323 (2025) 147211

Contents lists available at ScienceDirect

International Journal of Biological Macromolecules

journal homepage: www.elsevier.com/locate/ijbiomac

Modulation of potato starch gelatinization, rheological properties, and mechanical properties: the role of potato soluble dietary fiber with different molecular weights

Zhenzhen Zhang [a,b], Qiannan Liu [a,*], Ruixuan Zhao [a], Jing Li [a], Honghai Hu [a,*], Aurore Richel [b]

[a] Institute of Food Science and Technology, Chinese Academy of Agricultural Sciences, Integrated Laboratory of Potato Staple Food Processing Technology, Key Laboratory of Agricultural Product Processing and Storage, Ministry of Agriculture and Rural Affairs, Beijing 100193, PR China
[b] Department of Biomass and Green Technologies, Gembloux Agro-Bio Tech, Université de Liège, Passage des Déportés 2, Gembloux B-5030, Belgium

ARTICLE INFO

Keywords:
Starch gelatinization
Molecular weight
Rheology research

ABSTRACT

This study investigated the effect of the molecular weight (Mw) of potato soluble dietary fiber (PSDF) on potato starch (PS) gelatinization. Crude PSDF delayed gelatinization, and significantly improved the viscoelasticity and structure orderliness of the gel. However, PSDFs of different Mws had different effects on these physicochemical properties of PS. High-Mw PSDF (PSDF-H) mainly adhered to the surface of the starch granules, limiting their bursting and reducing their size, thereby decreasing starch viscosity and reducing its storage modulus and loss modulus. By contract, low-Mw PSDF (PSDF-L) significantly increased the gel's storage modulus and loss modulus, resulting in a more uniform and dense gel and enhancing compressive resistance by 35.7 %. Moreover, PSDF-L increased the lamellar thickness of starch granules and inhibited starch hydration, thereby increasing gelatinization onset temperature from 61.6 to 64.1 °C, whereas PSDF-H had no significant effect (from 61.6 to 61.8 °C). Therefore, PSDF-L was more effective than PSDF-H in delaying gelatinization. Furthermore, large amplitude oscillatory shear analysis indicated that the PSDF-L/PS gel possessed superior gel strength. These findings promote the high-value utilization of PSDF and elucidate how starch gelatinization and dietary fiber regulate the starch gelatinization and gel properties.

1. Introduction

Consumers have shown a preference for starch gel foods with a high moisture content, such as cold jelly [1] and Liangpi (a traditional Chinese food) [2], with distinctive chewy textures that depend on starch gelatinization and subsequent retrogradation [2]. A consecutive three-step mechanism occurs during starch gelatinization in the production process: water absorption, swelling, and eventually bursting out to form a gel. However, the utilization of natural starch is limited due to its susceptibility to instability under diverse temperature and shear conditions [3]. Other components in food, such as protein, fat, dietary fiber (non-starch polysaccharides), and phytochemicals will affect starch gelatinization [4]. Of these, non-starch polysaccharides are frequently used to modulate starch gel pasting, gelation, retrogradation, and structural properties of starch gels [5–7]. Several studies have demonstrated that more than one gel structure-enhancing mechanism within non-starch polysaccharides-starch systems [8]. According to previous research, scientists speculated that they mainly occur via two mechanisms: (1) non-starch polysaccharides adhere around the surface of starch granules, forming a physical barrier around the starch granules, and (2) the embedding of non-starch polysaccharides into starch granules effect limits the gelatinization [9,10]. However, only a limited number of studies have validated both mechanisms using specific methodologies. For example, Matignon et al. [11] investigated the interaction between carrageenan and adhered cross-linked waxy starch granules using a confocal laser scanning microscope (CLSM), while they quantified the residual carrageenan in solution through rheometer viscosity measurement. Chen et al. [12] demonstrated that pectin could adsorb onto and penetrate potato starch granules via pectin adsorption isotherms. Nevertheless, the current characterization methods have limitations, and few relevant studies have revealed the causes and influencing factors underlying the action mechanism of soluble dietary fiber embedded in starch pores. Some have proposed that macromolecular chains are capable of penetrating small pores under conditions of

* Corresponding authors.
E-mail addresses: liuqiannan@caas.cn (Q. Liu), huhonghai@caas.cn (H. Hu).

https://doi.org/10.1016/j.ijbiomac.2025.147211
Received 29 May 2025; Received in revised form 25 August 2025; Accepted 27 August 2025
Available online 28 August 2025

static diffusion or stretched flow fields, with lower molecular weight (Mw) chains exhibiting greater ease in this process [13]. Therefore, the Mw of dietary fiber may be a key factor influencing the "embedding" theory. Further exploration is required to determine how dietary fiber interacts with starch and understand its effect on the gelatinization process.

Mw of dietary fibers can influence their aggregation state in water and the hydration and thermal gelatinization of starch during processing [10,14]. Studies have shown that different Mws of highland barley non-starch polysaccharides have varying effects on the physicochemical properties of rice starch [15]; medium-Mw (1.58×10^5 Da) shiitake soluble dietary fiber can bridge starch chains, forming a rigid, ordered, three-dimensional network structure and solid materials with low fluidity [16]; low-Mw (5.67×10^4 Da) arabinoxylans can more effectively hinder wheat starch gelatinization [17]. During gelatinization, dietary fiber affects the network structure of the dietary fiber-starch mixture through physical entanglement and electrostatic adsorption [9,18]. This mechanism ultimately leads to the formation of a more ordered and compact gel matrix in systems compared to native starch [19]. Zhang et al. [15] thought that the lower Mw polysaccharides tend to align and bind more readily with amylopectin chains. Consequently, it is hypothesized that, soluble dietary fibers with varying Mws in the mixed system may lead to distinct starch-dietary fiber interaction mechanisms, resulting in starch paste in different states during gelatinization, thereby influencing the starch gelatinization process.

Potato starch (PS) has become the world's third-largest commercial starch, alongside corn and wheat starch [7]. Industrial potato processing—such as the manufacture of chips, fries, and mashed potatoes—generates a substantial amount of solid residue annually [20]. Starch production and other industries worldwide generate 70–140 million tons of potato peels, accounting for approximately 15 % to 40 % of the initial raw materials [21,22]. However, most of these residues are underutilized—mainly discarded in landfills—posing potential negative environmental impacts or used as low-value animal feed [20]. Potato soluble dietary fiber (PSDF), an important by-product of potato processing, is a high-quality dietary fiber that contains various oligosaccharides and non-starch polysaccharides, which can increase the viscosity of gastric contents, delay gastric emptying, and thus prevent a sharp rise in blood sugar after meals [23,24]. Lattimer et al. [25] recommended an average daily intake dose of 18 g soluble dietary fiber to lower fasting blood glucose. At present, potato dietary fiber is mainly used to improve the nutritional content of starch-based foods [19]. Previous studies have shown that PSDF inhibits amylose leaching and promotes molecular interactions during gelatinization [19,26]. However, the exact mechanisms involved in the interaction between PS and PSDF during gelatinization remain to be elucidated. In this study, a mixed system of PS and PSDF was used to explore the interactions between PSDF of varying Mws and PS during gelatinization as well as the impact of these interactions on the rheological properties and structural characteristics of the starch gel. This work aims to promote the high-value PSDF utilization by regulating the behavior of starch gel and enhancing its shear resistance.

2. Materials and methods

2.1. Materials

Potato starch (S112495; 11.91 % moisture, 87.37 % starch, 30.71 % amylose, 0.34 % ash, 0.20 % fat, and 0.18 % protein) was purchased from Aladdin Biochemical Technology Co., Ltd. (Shanghai, China). Crude potato soluble dietary fiber (PSDF-C), high Mw potato soluble dietary fiber (PSDF-H), and low Mw potato soluble dietary fiber (PSDF-L) were obtained from Atlantic potato peels. All chemicals were of analytical grade.

2.2. Preparation of PSDF

2.2.1. Preparation of PSDF-C

Potato peels (material-to-liquid ratio of 1:20) were immersed in water at 80 °C for 3 h to extract the PSDF. After cooling the extract to 60 °C, alkaline protease (BWZ7368–2016, 300–400 U/mL, 25 mL) was added for enzymatic hydrolysis at 60 °C for 30 min. The mixture was centrifuged and supernatant was concentrated to one-third of its original volume using rotary evaporation (50 °C, 0.09 MPa, 80 rpm). Then, the solution was then washed using Sevag reagent (chloroform and *n*-butanol mixed at a volume ratio of 4:1) with high-speed shaking. Subsequently, the mixture was centrifuged (8000 ×*g*, 5 min) to remove the precipitate (protein), and the supernatant was retained. This step was repeated 10 times to ensure the complete protein removal, followed by rotary evaporation to remove the organic solvents. The concentrate was re-dissolved by adding an equal volume of water, and any precipitate was removed by centrifugation (8000 ×*g*, 5 min). Subsequently, four volumes of 95 % ethanol were added to the supernatant, and the mixture was left to stand overnight. After another centrifugation at 8000 ×*g* for 5 min, the precipitate was frozen at −20 °C for 12 h and then lyophilized (0.01 atm, −60 °C, 24 h) to obtain freeze-dried PSDF-C.

2.2.2. Preparation of PSDF with different Mws

PSDF-C (2 g) was dissolved in 20 mL of distilled water to prepare a 0.1 g/mL solution. Subsequently, ethanol was added to the solution at different volume fractions of 10 %, 20 %, 30 %, 40 %, 50 %, 60 %, 70 %, and 80 % (*v*/v), with thorough mixing after each addition to ensure the mixture was homogeneous. After each ethanol addition, the solution was precipitated at 4 °C for 12 h. Precipitates were harvested by centrifugation at 14000 ×*g* for 5 min at 4 °C. The supernatant was carefully removed and the precipitates were collected. The precipitates with ethanol final volume of 40 % and 60 % were named PSDF-H and PSDF-L, respectively. Each sample was washed twice with 15 mL of 95 % ethanol and acetone, followed by lyophilization.

The Mws of PSDFs were determined using a gel permeation chromatographic system with a multi-angle laser light-scattering detector (MALS, Wyatt Technology DAWN EOS, California, USA). The chromatographic conditions were as follows: column: Shodex806; mobile phase: 0.1 M NaCl; flow rate: 0.5 mL/min; injection volume: 100 μL. As the ethanol concentration increased from 10 % to 80 %, Mw of corresponding PSDF subfractions gradually decreased. The precipitation behavior of carbohydrate in polar organic solvents was dependent on the molecular structure highly related to aqueous solubility (hydration) [27]. Therefore, the separation of these PSDF precipitates with different Mws was based on the different solubility in water/ethanol solutions at different ratios [28]. The Mw of PSDF-C is $peak_1 = 4.24 \times 10^4$ Da, $peak_2 = 3.70 \times 10^3$ Da, the Mw of PSDF-H is 4.97×10^4 Da, and the Mw of PSDF-L is 3.90×10^3 Da (Supplementary Table 1).

The total sugar, protein, and reducing sugar contents of the PSDFs were quantified using the phenol–sulfuric acid method, Coomassie Brilliant Blue staining, and the DNS method, respectively (Supplementary Table 1). Besides, chromatographic analysis was conducted to determinate their monose composition (Supplementary Table 1).

2.3. Preparation of different PSDF/PS mixture samples

2.3.1. Preparation of PSDF/PS suspensions

Based on the model with a starch–polysaccharide ratio of 10:1 [29], and considering that 10 % potato starch can form a stable gel, this study selected a 10 % (m/v) starch concentration and a 1 % (m/v) PSDF concentration. PSDFs were dissolved in deionized water to prepare 1 % PSDF-C, PSDF-H, and PSDF-L solutions. Then, 10 % PS was added to each PSDF solution and soaking for 1 h to form PSDF/PS suspensions.

2.3.2. Preparation of PSDF/PS paste

Four equal PSDF/PS suspension samples were simultaneously heated

from 25 to 95 °C at 1000 rpm using a ThermoMixer (Eppendorf AG, Hamburg, Germany). At each target temperature (65, 75, 85, and 95 °C), one sample was promptly removed for further analysis.

2.3.3. Preparation of PSDF/PS mixed gels

PSDF/PS suspensions were heated at 95 °C for 20 min with agitation at 1000 rpm. After that, the tubes were equilibrated for 20 h at 4 °C to form PSDF/PS mixed gels (30 × 10 mm). After freeze-drying these gels and grinding them into powder, they were passed through a 120-mesh sieve to obtain lyophilized PSDF/PS powder.

2.4. Confocal laser scanning microscopy (CLSM)

The relationship between starch granules and PSDF in the PSDF/PS suspensions was observed using a CLSM (LSM T-PMT 880; Carl Zeiss, Germany) equipped with a 40 × objective [30]. Nile blue A (0.05 %, w/v) and fluorescein isothiocyanate (FITC, 0.10 %, w/v) were prepared to locate PS and PSDF in the sample. In brief, 10 μL of Nile blue A solution was added to 1 mL of 10 % PSDF/PS suspension. After 5 min of dyeing via shaking, 10 μL of FITC was added to the suspension for 1 min and observed immediately. As the two dyes formed covalent bonds with target molecules, they will not cross-color during this a short period. A droplet of the dye sample was drawn using a disposable plastic pipette, was placed on the slide and covered with a cover slip. Its edges were sealed with glycerol diluent to prevent moisture evaporation. PS (red) and PSDF (green) were visualized using excitation wavelengths of 638 and 495 nm, respectively.

2.5. Small angle X-ray scattering (SAXS)

The influence of the presence of PSDF before and during gelatinization on the supramolecular structure of PS was observed by SAXS (Anton Paar SAXS point 2.0, Austria). The 10 % PSDF/PS suspensions were thoroughly mixed, soaked for 12 h at 4 °C, and then repeatedly washed with deionized water (≥10 times). Starch particles were collected and dried at 45 °C. The starch samples were then formulated into a 50 % (w/v) suspension and soaked for 12 h at 4 °C. Finally, the starch sediment and PSDF/PS pastes (prepared under different temperature conditions) were respectively loaded into a specialized sample holder for SAXS testing. Each sample was prepared in triplicate.

X-ray diffraction was performed using a Cu-Kα X-ray (λ = 0.154 nm) operated at 50 kV and 0.6 mA with an exposure time of 6 min [31]. Background scattering and smeared intensity were removed by using SAXSquant 3.0 to analyze the SAXS data. A one-dimensional scattering curve representing the variation in scattering intensity (I) as a function of the scattering vector (q) was generated and normalized.

Bragg's law (Eq. (1)) was applied to determine the periodic thicknesses of the amorphous and crystalline lamellae in each set of samples:

$$d_{Bragg} = 2\pi/q \quad (1)$$

where d_{Bragg} represents the periodic thickness and q represents the scattering vector of the scattering peak in the scattering curve.

2.6. Optical microscopic observation of the appearance of starch granules

One drop from each PSDF/PS paste prepared under different temperature conditions was immediately transferred onto individual microscope slides. An iodine solution was then added to each slide and subsequently rinsed with distilled water. The edges of the slides were sealed with a glycerin–water (1:1) mixture. The prepared slides were examined under an optical microscope at 10× magnification to visualize the samples [32].

2.7. Size distribution and zeta potential analysis

Particle size distribution and zeta potential of the starch paste after adding PSDFs were observed. Two mL of the PSDF/PS pastes prepared under different temperature conditions were diluted to 10 mL with deionized water and agitated at 1000 rpm for 6 h to ensure homogeneity. The particle size distribution was measured using a laser particle size analyzer (Microtrac Inc., Montgomeryville, PA, USA). The volume-based mean diameter (D[4,3]) and area-based mean diameter (D[3,2]) of the starch were recorded, with refractive indices set to 1.33 for water and 1.53 for starch [33]. The zeta potential of the PSDF/PS pastes was measured by a zeta potential analyzer (Zetasizer Nano-ZS90, Malvern Instruments, Malvern, UK) at 25 °C. Each test was conducted in triplicate.

2.8. Pasting properties and content of leached amylose

The pasting properties of starch samples were measured using a Rapid Viscosity Analyzer (RVA) (TecMaster, Perten, Australia). PS (1.5 g, dry base) was added to 25 mL of 1 % PSDF to prepare 6 % PSDF/PS suspension. The PSDF/PS suspension was equilibrated at 50 °C for 2 min, heated to 95 °C for 2.5 min at 12 °C/min, cooled to 50 °C at 12 °C/min, and maintained for 2 min. The stirring speed was 960 rpm for the first 10 s, after which it was decreased to 160 rpm. The peak viscosity (PV), trough viscosity (TV), breakdown (BD), final viscosity (FV), and setback (SB) of the PSDF/PS suspension were determined from the viscographs.

The content of leached amylose was determined using an amylose content assay kit (Boxbio Science and Technology Co., Ltd., Beijing). Briefly, 10 mg of the sample was mixed uniformly in 5 mL of deionized water, then heated at 95 °C for 10 min, equilibrated at room temperature, and centrifuged at 4000 ×*g* for 5 min. The amount of amylose leaching in the supernatant was determined using the kit.

2.9. Thermodynamic properties

The thermal transition temperatures of the starch samples were measured using a Q200 differential scanning calorimeter (DSC, TA Instruments Inc., New Castle, DE, USA). Specifically, 3 mg of PS and 10 μL of 1 % PSDF were mixed in an aluminum pan and stored overnight at 4 °C. The mixture was then transferred to the DSC and scanned over a temperature range of 30–100 °C at 5 °C/min.

2.10. Rheological properties

The rheological properties of the PSDF/PS mixture (prepared as described in Section 2.8) were evaluated using a rotational rheometer (Netzsch Kinexus Lab$^+$, Netzsch Scientific Instruments Inc., Germany) at 25 °C (gap,1 mm; probe, P50, 50 mm) [34]. After loading the sample, silicone oil was used for edge sealing to prevent water evaporation. The linear viscoelastic region (LVR) was identified by varying the strain from 0.1 % to 1000 % at 1 Hz. To investigate the functional relationships between stress and applied strain during the instantaneous deformation period (stress–strain curves), a large amplitude oscillatory shear (LAOS) analysis was conducted at 1 Hz, with the shear strain varied within the range of 0.1 % to 100 %. The apparent viscosity of all samples was determined over a shear rate range of 0.1 to 100 s^{-1}. Frequency sweeps were tested within the range of 0.1 to 100 Hz at 0.1 % strain, and recorded the results of storage modulus (G') and loss modulus (G").

2.11. Microstructure

The gel cross-sectional morphology was characterized using a JSM-6700F scanning electron microscope (SEM; Hitachi, Tokyo, Japan) operated at 10 kV and 100 × magnification.

2.12. Fourier transform infrared spectroscopy (FTIR)

The FTIR spectra of the PSDFs and lyophilized PSDF/PS powder were acquired using a Thermo Nicolet 67 FTIR spectrometer (TENSOR 27; Bruker, Billerica, MA, USA) from 4000 to 400 cm^{-1}. The samples were combined with KBr (PSDF/PS powder: KBr = 1:100), pressed into pellets, and scanned approximately 64 times.

2.13. X-ray diffractometry (XRD)

The relative crystallinity of the lyophilized PSDF/PS powders was evaluated using a Dmax 2500 PC X-ray diffractometer (Rigaku Corporation, Tokyo, Japan) with Cu Kα radiation (λ = 0.154 nm) at 40 kV and 30 mA. Scans were performed from 4° to 35° 2θ at 2°/min and a step size of 0.02°. Each test was repeated five times.

2.14. Distance-stress transfer curve

Compression testing of PSDF/PS mixed gels was performed using a Texture Analyzer (CT3–10 kg, Brookfield, MA, USA). The test parameters were as follows: probe TA25/1000; stamping depth, 3 mm; trigger point 5 g; forward rate, 2 mm/s; stamping rate, 1 mm/s; and retracting rate, 2 mm/s [35].

2.15. Statistical analysis

All experiments were repeated at least three times, and the mean ± standard deviation was calculated. Statistical analysis was performed using one-way ANOVA followed by Duncan's test in SPSS (version 23.0; SPSS Inc., Chicago, IL, USA) when *P*-values < 0.05. Figures were created using Origin 2018 software (OriginLab, Northampton, MA, USA).

3. Results and discussion

3.1. State of PS and PSDF in water before gelatinization

The coexistence of PS and PSDF in the suspension was observed by CLSM (Fig. 1A). When PS and PSDF were mixed, the PSDF was observed to adhere to the starch shell. Consistent with previous studies, non-starch polysaccharides attached to the PS surface the starch micropores of starch particles [5,12,19]. Other studies have shown that polysaccharides on the starch particle surface can interact with the starch granules through hydrogen bonds [36,37].

The SAXS spectrum of starch granules was observed (Fig. 1B). A distinctive scattering peak of PS appeared at a scanning intensity (q) of 0.71 nm^{-1}, corresponding to a periodic length of 8.81 ± 0.00 nm, as calculated using Bragg's law [38]. Following infiltration with PSDF and washing to remove unbound PSDFs, all PS scattering peaks showed a noticeable leftward shift. The SAXS peaks position was related to the overall thickness of the crystalline and amorphous regions within the layered structure of starch [39]. A smaller layer thickness indicated a higher degree of structural order [39]. After adding PSDF-L, PS was observed to significantly increase the layer thickness (9.03 ± 0.02 nm), suggesting that the arrangement of the crystalline layers and semi-crystalline growth rings became more loosely organized. Presumably, PSDF promoted partial dissociation of the double helix, resulting in loosening the system [40]. Therefore, PSDF-L might permeate the starch granules and significantly disrupt the layered structure of starch.

3.2. Thermodynamic properties of PSDF/PS mixtures

DSC analysis revealed the thermodynamic attributes of the PSDF/PS composites. As detailed in Table 1, the critical parameters included onset temperature (To), peak temperature (Tp), conclusion temperature (Tc), and enthalpy change (ΔH).

Compared with native PS, the To and Tp value of PSDF-C/PS (the mixture of crude potato soluble dietary fiber and potato starch) and PSDF-L/PS (the mixture of low molecular weight potato soluble dietary fiber and potato starch) increased, whereas the paste temperature of PSDF-H/PS (the mixture of high molecular weight potato soluble dietary fiber and potato starch) did not substantially change. Liu et al. [41] posited that the increase in transition temperatures was primarily due to the hindrance of hydration interactions between starch and water molecules. Therefore, PSDF-L predominantly restricted starch hydration, thereby delaying the gelatinization process, which subsequently

Table 1
Thermal properties of PSDF/PS mixtures.

	PS	PSDF-C/PS	PSDF-H/PS	PSDF-L/PS
To	61.6 ± 0.1^{c}	62.2 ± 0.1^{b}	61.8 ± 0.1^{bc}	64.1 ± 0.4^{a}
Tp	64.6 ± 0.2^{c}	65.3 ± 0.1^{b}	64.8 ± 0.2^{c}	66.4 ± 0.3^{a}
Tc	68.6 ± 0.3^{b}	68.8 ± 0.1^{b}	68.3 ± 0.3^{b}	70.1 ± 0.9^{a}
ΔH	9.553 ± 0.5^{a}	7.961 ± 0.6^{b}	8.624 ± 0.3^{b}	8.602 ± 0.1^{b}

Note: values with different letters in the same line are significantly different with P<0.05.

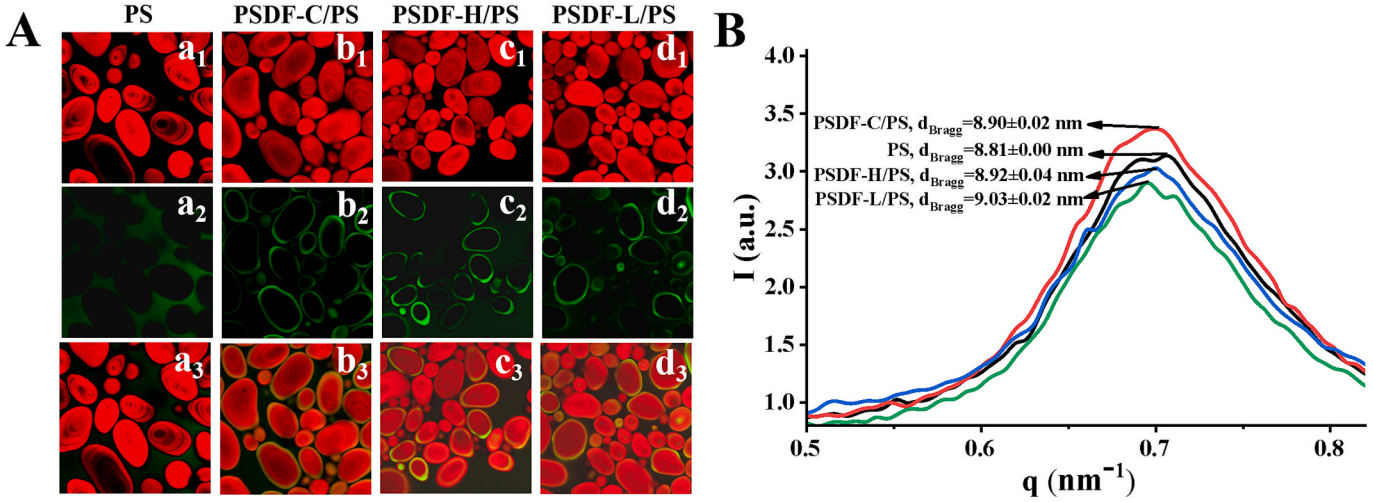

Fig. 1. Images of PSDF/PS suspension before gelatinization by CLSM (A) and SAXS spectra of washed PSDF/PS granules (B). a_1-a_3: PS suspension; b_1-b_3: PSDF-C/PS suspension; c_1-c_3: PSDF-C/PS suspension; d_1-d_3: PSDF-L/PS suspension; red represents PS and green represents PSDFs (Fig. 1A). (For interpretation of the references to color in this figure legend, the reader is referred to the web version of this article.)

required higher temperatures for phase transition and enhanced thermal stability [31]. Through pectin adsorption isotherms, Chen et al. [12] demonstrated that pectin adheres to the surfaces of potato starch, pea starch, and rice starch. However, the addition of pectin had no significant effect on the To value of these three starches. Therefore, it was speculated that even if PSDF-H adheres to the surface of starch, it does not significantly limit the hydration of starch. ΔH represents the energy demand for starch gelatinization and reflects the efficiency of the process. As shown in Table 1, PSDF significantly decreased the ΔH of PS. Combined with SAXS results, it is likely occurred due to interactions between PSDF and starch molecules, which disrupted the layered structure of starch and made its structure looser.

3.3. Leached amylose content and pasting properties

The addition of PSDF during PS gelatinization gradually decreased the amount of leached amylose from 31.7 ± 0.5 to 26.3 ± 0.6 mg/g (Table 2). PSDF-L exhibited a more pronounced inhibitory effect than PSDF-H, indicating that PSDF effectively inhibited amylose leaching during gelatinization. This phenomenon might have occurred because PSDF-L limited the hydration interactions between starch and water molecules, thereby markedly restricting starch expansion and reducing amylose leaching. Furthermore, as described in Section 3.2, PSDF-L dramatically delayed gelatinization by inhibiting amylose leaching.

As shown in Fig. 2, PSDF reduced the PV, BD, and TV values of the PSDF/PS composites. The PV is comprehensively influenced by several factors, including the extent of amylose leaching, granule swelling, friction between swollen granules, and free water competition [42]. The decreases in PV and BD indicated that PSDF may impede granule swelling and enhance starch thermal and shear resistance. In addition, the SB value of PSDF-C/PS and PSDF-L/PS increased, indicating that PSDF-C and PSDF-L accelerated the short-term retrogradation of the PSDF/PS paste. The influence of dietary fibers on starch retrogradation is complex, and contradictory findings have been published in this regard [43]. The decrease in the SB value of the PSDF-H/PS paste indicated that PSDF-H inhibited the short-term starch retrogradation. Kong et al. surmised that this phenomenon may be due to interactions between the leached amylose and the dietary fiber, which interfere with the hydrogen bonding interactions between amylose molecules [44].

3.4. Starch particles changes in PSDF/PS mixtures during gelatinization

Changes in the morphology, size, and molecular structure of starch particles during gelatinization were observed using iodine staining, laser particle size analysis, and SAXS (Table 3 and Fig. 3). Upon heating, the starch granules gradually hydrated and swelled. As the temperature increased, the starch granules burst into fragments and became increasingly transparent (Fig. 3A), which was attributed to order structure disruption, enabling amylose to leach gradually. Further analysis of Fig. 3B revealed that the crystalline regions of starch were destroyed during gelatinization, and the electron density between crystalline and amorphous lamella decreased.

At the initial stage of gelatinization (65 °C), the D[4,3] and D[3,2] values of the PSDF-C/PS and PSDF-L/PS mixed systems were significantly lower than those of the PS and PSDF-H/PS systems (Table 3). The results showed that, after the addition of PSDF-C and PSDF-L, the starch granules in the mixture were smaller than those in the pure starch at the same temperature. Moreover, the PSDF-H/PS diffraction peak intensity was similar to that of PS, whereas the diffraction peak intensities of PSDF-C/PS and PSDF-L/PS were stronger (Fig. 3B). This phenomenon was consistent with the DSC results, which illustrated PSDF-L can more easily restricted the starch hydration and the interaction between PS and PSDF-L can affect the starch gelatinization process, thus increasing the gelatinization temperature and delaying starch gelatinization.

When the heating temperature reached the melting temperature of starch, the ordered arrangement of the crystal and amorphous lamellae was lost, resulting in the disappearance of the scattering peak of the gelatinized starch [45]. However, during the middle stage of gelatinization (75 °C and 85 °C), the D[4,3] and D[3,2] values of the PSDF-H/PS system were significantly smaller than those of the other groups, indicating that PSDF-H inhibited further starch expansion or limited the size of starch fragments after the starch granules ruptured (Table 3). This reduction suggested that PSDF restricted starch granules expansion, possibly due to PSDF coating the surface of starch granules (Fig. 1A). Although all PSDFs could adhere to the surface of starch, while PSDF-H had better organization and inter-chain associations and was more likely to form a network structure [16]. Moreover, compared with PSDF-C/PS and PSDF-L/PS, the D[4,3] and D[3,2] of PSDF-H/PS at 75 °C and 85 °C were significantly smaller. This may have been due to the inhomogeneous attachment of PSDF-H molecules to the granule surface, with some areas expanding more than others [46]. When the granules continued to expand upon heating, the coating layer may have caused the granules to break at certain weak points, resulting in smaller fragments. A similar phenomenon was observed by Kong et al. when adding cordyceps sinensis polysaccharides (1.273×10^3 Da) to wheat starch [44].

As shown in Fig. 3A, PS was completely broken down into irregular flaky shapes after gelatinization, rather than retaining a swollen granule. This observation indicated that all starch granules underwent gelatinization during the heating process in water. Conversely, with the addition of PSDF-L, some starch granules remained intact or were only partially broken. This result strongly illustrated that the PSDF-L could delay PS gelatinization, which was consistent with the DSC test results.

3.5. Zeta potential of PSDF/PS paste

Zeta potential was measured to evaluate system stability by detecting the particle surface charges; the zeta potential of the PSDF/PS paste is shown in Fig. 4. The zeta potential of PS was −1.59 mV, likely due to ionization of hydroxyl groups on starch molecular chains, generating a negative charge. All PSDFs carried a negative charge (Supplementary Table 1). After the addition of PSDFs, the absolute value of the zeta potential of the PS paste increased. This was because PSDF had a multi-hydroxyl structure with many free hydroxyl groups. Compared with PS, the PSDF-L/PS mixture had the highest absolute value of zeta potential (−5.67 mV). The surface charge on particles determines their dispersion and aggregation. Generally, the higher the absolute value of the zeta potential value, the greater the electrostatic repulsion between particles, leading to more uniform dispersion, reduced aggregation tendency, and enhanced system stability [47]. Addition of PSDF-L increased the zeta

Table 2
The amount of leached amylose and pasting characteristics of PSDF/PS mixtures.

	PS	PSDF-C/PS	PSDF-H/PS	PSDF-L/PS
Leached amylose (mg/g)	31.7 ± 0.5^{a}	28.1 ± 0.8^{bc}	28.8 ± 1.4^{b}	26.3 ± 0.6^{c}
PV/mPa·s	4857.5 ± 9.2^{a}	1947.5 ± 36.1^{b}	1979.0 ± 1.4^{b}	1934.0 ± 22.6^{b}
TV/mPa·s	1618.0 ± 33.9^{a}	1265.5 ± 17.7^{c}	1397.5 ± 17.7^{b}	1151.0 ± 7.1^{d}
BD/mPa·s	3239.5 ± 24.7^{a}	682.0 ± 18.4^{c}	581.5 ± 16.3^{d}	783.0 ± 29.7^{b}
FV/mPa·s	1786.5 ± 30.4^{a}	1524.0 ± 52.3^{b}	1686.5 ± 37.5^{a}	1266.5 ± 31.8^{c}
SB/mPa·s	168.5 ± 3.5^{b}	258.5 ± 34.6^{a}	115.5 ± 38.9^{b}	289.0 ± 19.8^{a}

Note: values with different letters in the same line are significantly different with $P < 0.05$.

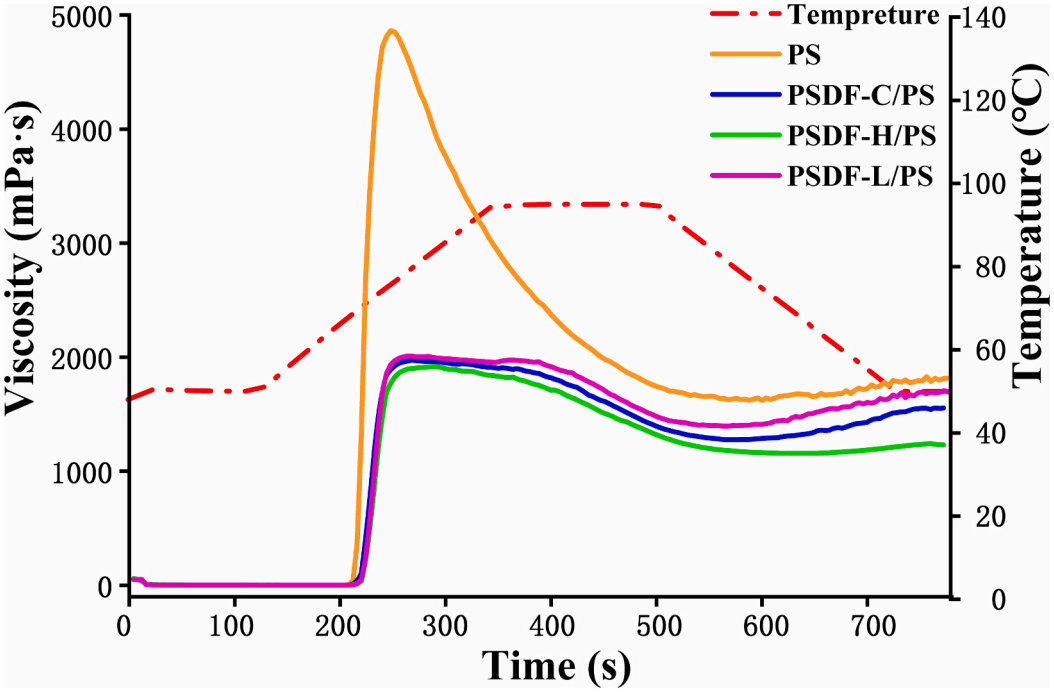

Fig. 2. Pasting profiles of PSDF/PS mixtures.

Table 3
D[4,3] and D[3,2] of PSDF/PS mixtures.

		PS	PSDF-C/PS	PSDF-H/PS	PSDF-L/PS
D[4,3]	65 °C	101.5 ± 2.1^{a}	51.3 ± 2.2^{c}	103.0 ± 1.4^{a}	62.8 ± 0.3^{b}
	75 °C	217.1 ± 5.5^{a}	146.5 ± 0.5^{b}	126.5 ± 8.3^{c}	147.2 ± 8.8^{b}
	85 °C	167.7 ± 4.6^{a}	137.7 ± 2.1^{c}	87.2 ± 2.6^{d}	149.6 ± 1.9^{b}
	95 °C	109.8 ± 1.1^{a}	83.8 ± 4.4^{b}	78.2 ± 1.2^{b}	114.4 ± 2.0^{a}
D[3,2]	65 °C	54.5 ± 0.7^{b}	41.0 ± 0.3^{d}	64.7 ± 0.4^{a}	45.8 ± 0.7^{c}
	75 °C	137.8 ± 0.3^{a}	96.8 ± 2.5^{b}	65.5 ± 1.5^{d}	89.8 ± 1.4^{c}
	85 °C	107.6 ± 0.1^{a}	90.0 ± 0.9^{c}	50.8 ± 0.2^{d}	96.7 ± 3.2^{b}
	95 °C	79.4 ± 1.6^{a}	54.5 ± 2.8^{b}	47.8 ± 0.8^{b}	54.0 ± 2.0^{c}

Note: values with different letters in the same line are significantly different ($P<0.05$).

potential significantly, enhancing electrostatic repulsion between particles and preventing further aggregation. PSDF affected the aggregation and gel properties of starch particles to some extent through electrostatic interactions, and the mixed system achieved the highest stability when PSDF-L was added [48]. This may be due to the small molecular size and the small z-average root-mean-square radius of gyration (Supplementary Table 1) of PSDF-L, which is more likely to adhere to the starch side chains due to its small steric hindrance than PSDF-H, thus effectively affecting the electrostatic interactions between starch molecules during gelatinization [17,35]. Furthermore, this interaction may improve the association between starch molecules and PSDF chains during gelatinization, thus improving the starch molecular order [49].

3.6. Rheological properties of PSDF/PS mixed gels

Fig. 5 summarized a comprehensive analysis of the rheological properties of the PSDF/PS gel system. The apparent viscosity of all samples decreased sharply with an increasing shear rate, demonstrating pronounced shear-thinning behavior. Under shear stress, entangled and aggregated starch chains were separated, leading to reduced shear resistance [50]. Within the LVR, the G′ values of all PS gels was significantly higher than the G″ values, and the tan δ values of all gels were less than 1, indicating their superior elastic characteristics. As shown in Fig. 5C, the G′ and G″ values of the PSDF-C/PS and PSDF-L/PS gels were significantly higher than those of the PS gel. Moreover, a lower tan δ value (indicating a more rigid and structured and less viscous material) was achieved for PS in the presence of PSDF-C and PSDF-L, which was indicative of a stronger three-dimensional network due to impregnation by these two types of fibers [51]. However, the viscosity and G′ and G″ values of the PSDF-H/PS gel decreased significantly, suggesting that PSDF-H weakened the viscoelastic properties of the gels. This could be attributed to PSDF-H inhibiting the short-term retrogradation of PS (Section 3.3), thereby reducing molecular entanglement and interactions within the system and enhancing liquidity while decreasing the overall viscosity [34].

Within the LVR, the oscillation stress response is sinusoidal. By contrast, under the nonlinear regime, the viscoelastic modulus largely depends on the imposed strain, and the existence of higher harmonics in the stress response results in distorted, non-sinusoidal shear stress waveforms [52]. Within a strain amplitude of up to 10 %, the stress–-strain curves of all samples exhibited a narrow spindle shape, suggesting that the linear elastic solid-like behavior of all gels was excellent [53,54]. The low hysteresis loop area of the PS and PSDF-H/PS gels indicated low microstructural elasticity, which rendered these gels more susceptible to rupture under a large degree of deformation and consequently led to a more pronounced nonlinear response [54]. As the strain increased, the elliptical shape began to distort (40 % and 100 % strain), and both the degree of deformation and the enclosed area of the loop gradually increased with increasing strain. When the strain reached 40 %, the hysteresis loop of the PSDF-L/PS gel still maintained a spindle shape, whereas the others all underwent deformation. When the strain reached 100 %, the spindle-shaped hysteresis loop of the PSDF-L/PS gel showed slight deformation, whereas those of the other gels became more significantly deformed, tending toward a parallelogram. This indicated that viscous dissipation increased during the periodic deformation process, and the material transitioned from being predominantly elastic to viscous [53,55].

Notably, although the PSDF-C/PS and PSDF-L/PS gels showed relatively similar degrees of linear viscoelasticity in the LVR (Fig. 5C), they exhibited significantly different nonlinear viscoelastic responses under LAOS testing. The hysteresis loop of the PSDF-C/PS gel exhibited a more pronounced torsion effect, with deformation occurring earlier than in

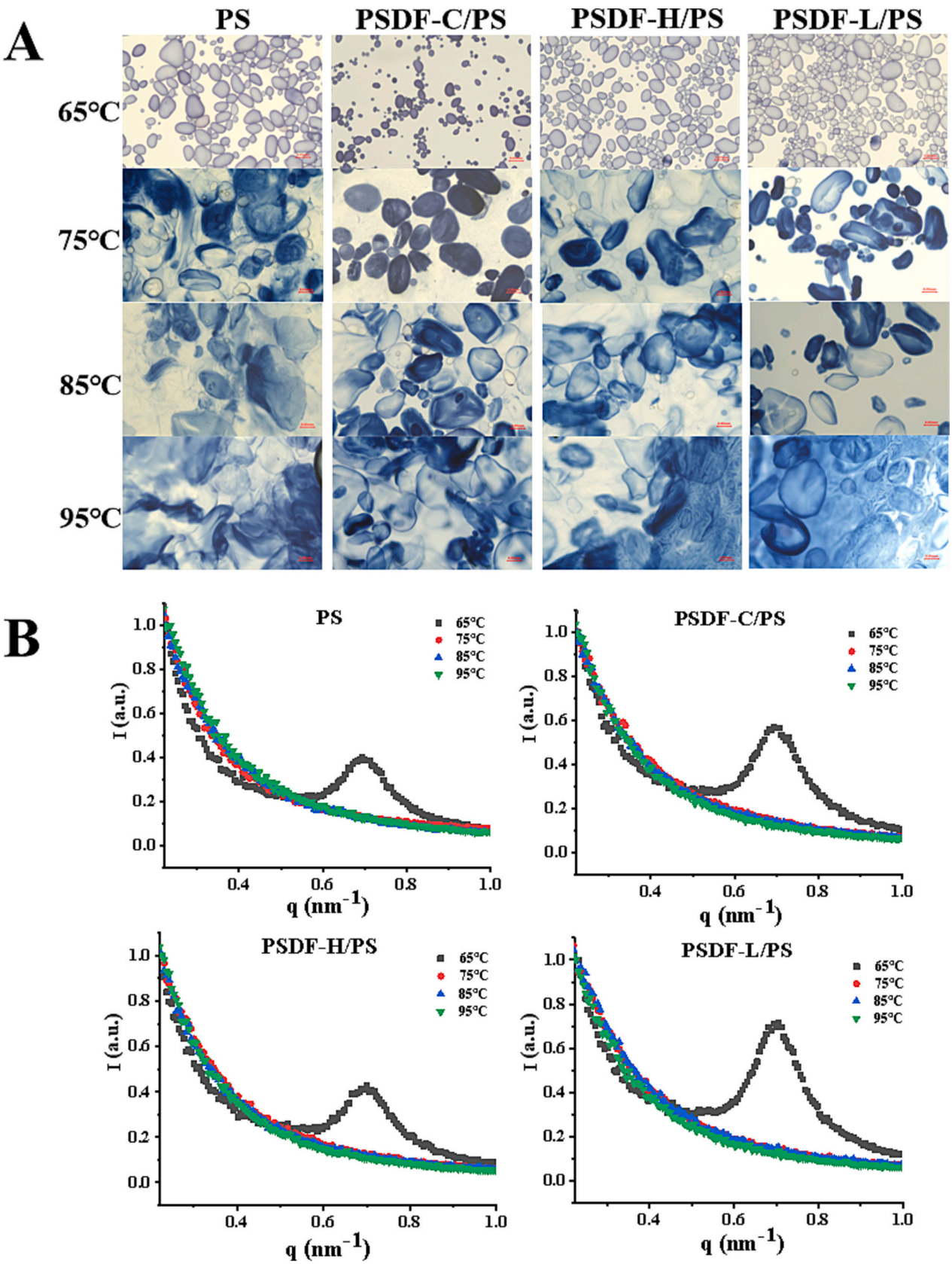

Fig. 3. Particle changes (A) and SAXS spectra (B) of PSDF/PS paste during gelatinization.

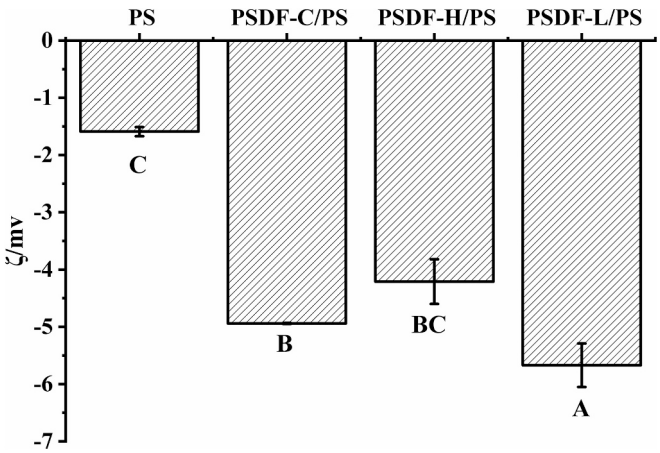

Fig. 4. Zeta potential of PSDF/PS paste. Different letters on error bars indicate significant differences ($P < 0.05$).

the case of the PSDF-L/PS gel. This may be attributed to the ability of PSDF-L to stabilize the gel system ($\zeta = -5.67$ mV) and stronger interactions with the starch molecules are formed, thereby reinforcing the overall gel structure [56]. This phenomenon provides more useful information for determining the structural changes under large degrees of deformation and the practical processing and application of starch gels. Consequently, the PSDF-L/PS mixture exhibited superior gel strength and greater resistance to permanent deformation.

3.7. Microstructure of PSDF/PS mixed gels

The microstructures of the PSDF/PS mixed gels were characterized using SEM. The pores in the gel structure reflect the initial distribution of water molecules within the network prior to drying for SEM analysis. During the cooling process, the starch molecules underwent rearrangement and aggregation, resulting in the formation of a dense gel network. The higher density of homogeneous pores indicated that higher water dispersion occurred throughout the network and that the network structure was denser. As shown in Fig. 6, compared with PS gel, the addition of PSDF-C reduced the gel pores and porosity of PSDF-C/PS gel, resulting in a denser gel network. Furthermore, after the addition of PSDF-H and PSDF-L, particularly PSDF-L, the pore distribution interval became narrower, indicating an increased degree of order in the PSDF-L/PS gel network. This observation also confirmed the enhanced stability of the PSDF-L/PS mixture, as evidenced by the zeta potential measurements. This indicates that PSDF-L could help mitigate the fragility of high-moisture starch gel products caused by an uneven interchain structure.

3.8. Changes in molecular structure of PSDF/PS mixed gels

Fig. 7 presented the FTIR and XRD spectra of the PSDF/PS mixed gels. As shown in Fig. 7A, the peak at 2926 cm^{-1} corresponds to the C—H_2 antisymmetric stretching vibrations and the C—H stretching vibrations. The peak at 1080 cm^{-1} is caused by the bending vibration of the C—H bonds. Additionally, the peak at 996–1000 cm^{-1} is associated with the bending vibrations of C-OH bonds. The particularly strong absorption peak at 3380 cm^{-1} resulted from O—H bond stretching vibrations and reflected both intramolecular and intermolecular hydrogen bonding [57,58]. Following the addition of PSDF, the absorption peak at 3380 cm^{-1} became broader, confirming that the hydrogen-bonding interactions between PSDF and PS increased [50,59]. The addition of PSDF did not alter the B-type configuration but intensified the diffraction peak intensity of starch at 17° (Fig. 7B).

The changes in the short-range ordered structure of starch (R 1045/1022) are closely related to changes in helical structures [31]. Relative crystallinity, an indicator of the long-range order in starch, reflects changes in the proportion of crystalline and amorphous regions [60]. As depicted in Fig. 7, PSDF markedly increased both the short-range order degree and relative crystallinity of starch, and these values of PSDF-H/PS gel were both maximal (1.757 ± 0.04 and 38.93 ± 1.21 %). Combined with the RVA results, PSDF facilitated the entanglement and rearrangement of starch chains, and interactions between starch and PSDF molecular chains during cooling, thus enhancing the gel's short-range order degree and relative crystallinity. However, due to its small steric hindrance, PSDF-L might adhere to the starch side chains, impede the interaction between starch molecules, and limit amylose reorganization, thus decreasing the PSDF-L/PS gel's short-range order degree and relative crystallinity [60].

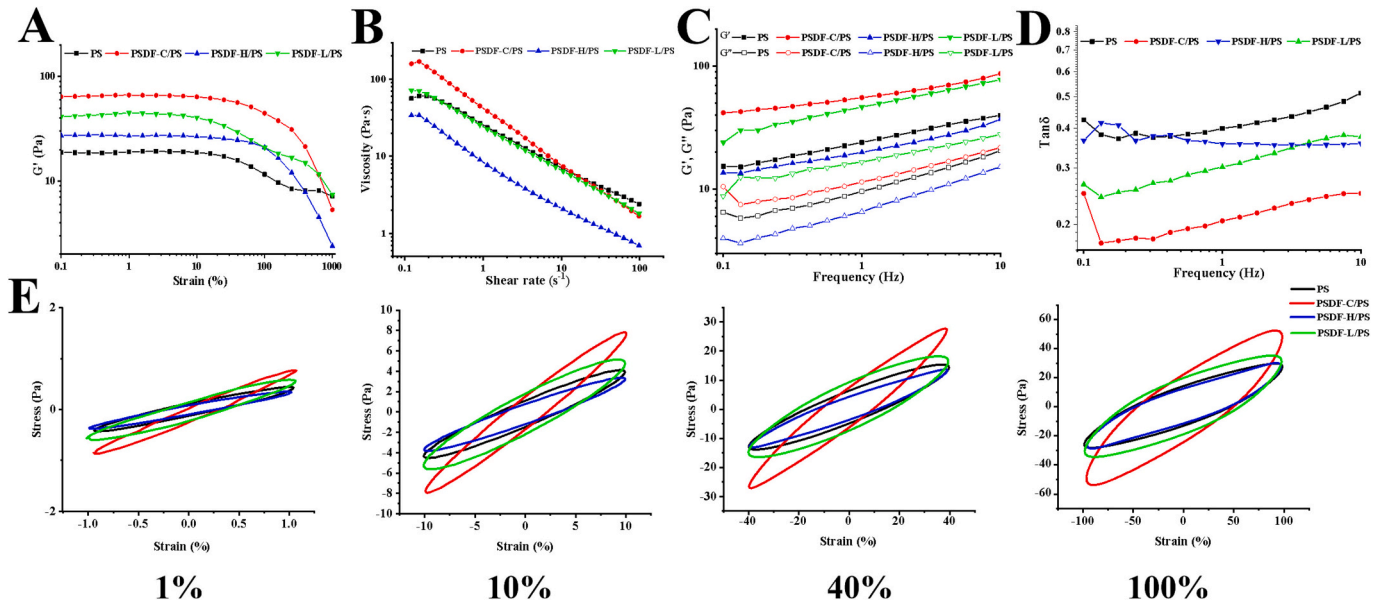

Fig. 5. Rheological properties of PSDF/PS mixed gels. A, stress scanning curve; B, viscosity curve; C: storage modulus (G') and loss modulus (G''); D: loss tangent modulus (tan δ); E: stress-strain curves of the mixed gels at different strains (1 %, 10 %, 40 %, and 100 %).

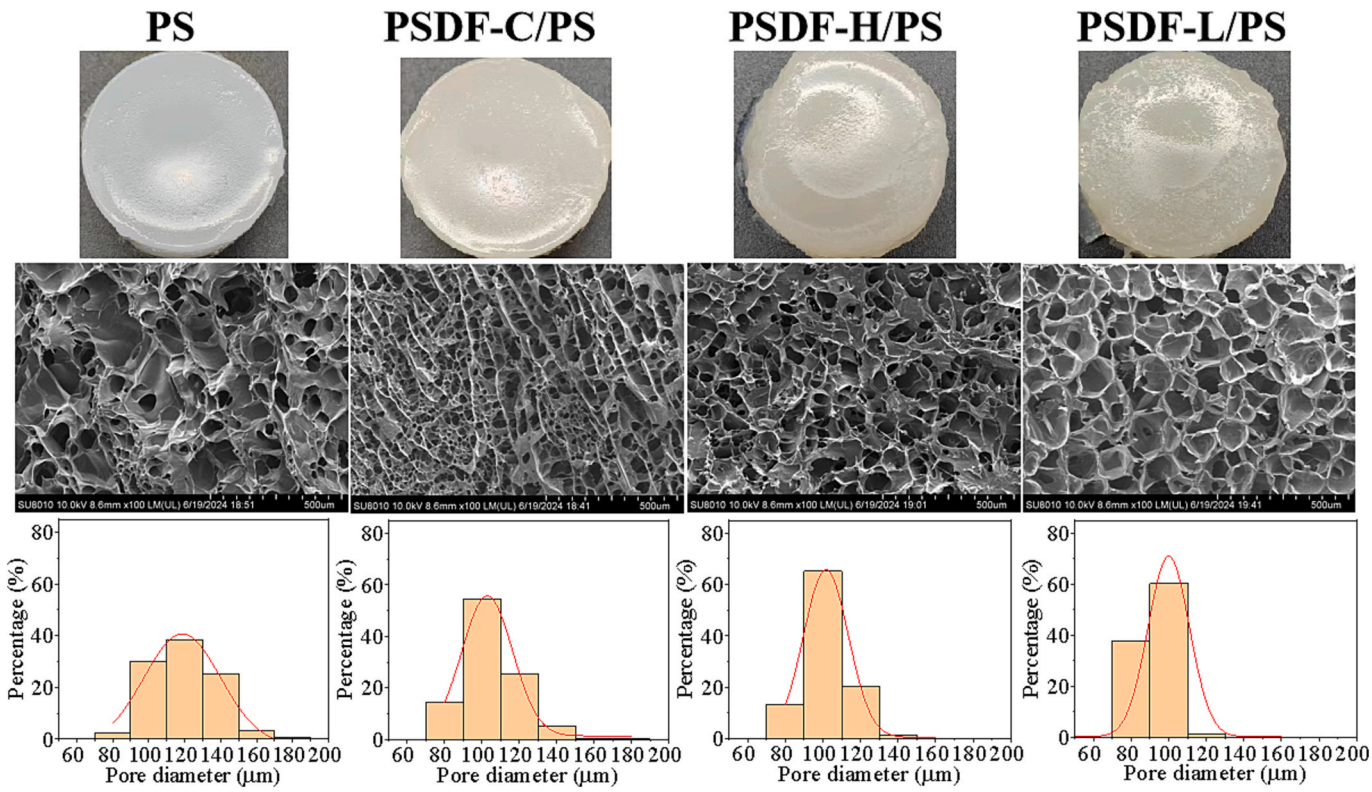

Fig. 6. Microstructure of PSDF/PS mixed gels (×100).

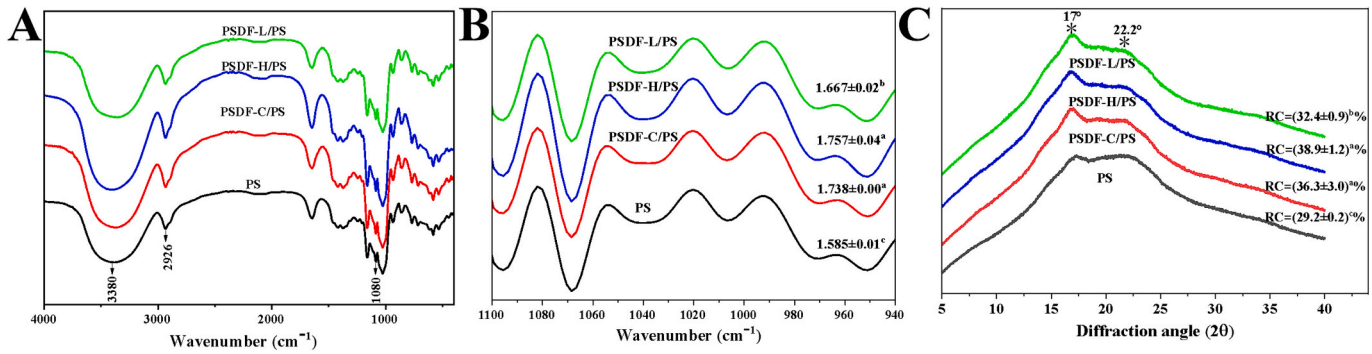

Fig. 7. FTIR spectra (A), deconvolution integration plots (B), and XRD patterns (C) of PSDF/PS mixed gels. RC: relative crystallinity.

3.9. Distance-stress transfer curve of PSDF/PS mixed gels

To investigate the impact of adding different Mw PSDFs on the rigidity of PS gel, the distance–stress transfer curves for the PSDF/PS mixed gels were recorded (Fig. 8). The addition of PSDF caused an upward shift in the distance–stress transfer curves of the mixed gels, indicating an improvement in the stiffness of the network structure of the PSDF/PS mixed gel. Compared to the PS gel, the gel stiffness of PSDF-C/PS and PSDF-L/PS increased by 23.8 % and 35.7 %, respectively. However, when PSDF-H was added, the deformation distance of the PSDF-H/PS gel shifted to the right, while rebound stress decreased, indicating a major reduction in the deformation resistance of the gel network structure. In contrast, the addition of PSDF-L resulted in a leftward and upward movement of the distance–stress transfer curve of the mixed gel, suggesting a significant enhancement in both the rigidity of the gel network structure and its deformation resistance. Fortunately, these results were consistent with the rheological results (Section 3.6). These findings may be attributed to the significantly more ordered three-dimensional network structure of the PSDF-L/PS mixed gel compared with that of the PSDF-H/PS mixed gel (Fig. 6). Therefore, PSDF-L has the potential to enhance the shear resistance of starch gel foods.

3.10. Interaction mechanism of PSDF and PS during gelatinization

Based on these results, a schematic model of the interaction between PSDF and PS during gelatinization was proposed (Fig. 9). Upon heating starch in excess water, it underwent gradual hydration and expansion, accompanied by the leaching of amylose and the disintegration of granules into fragments. PSDF restricted amylose leaching, thereby influencing starch gelatinization. The interaction mechanism between PSDF and starch varied depending on the Mw of PSDF. PSDF-H primarily formed a physical barrier by encapsulating the surface of PS granules, limiting their bursting and resulting in smaller starch fragments. Conversely, PSDF-L restricted the hydration and expansion of water molecules within starch, thus delaying the gelatinization process. Furthermore, during cooling, the addition of PSDF enhanced the

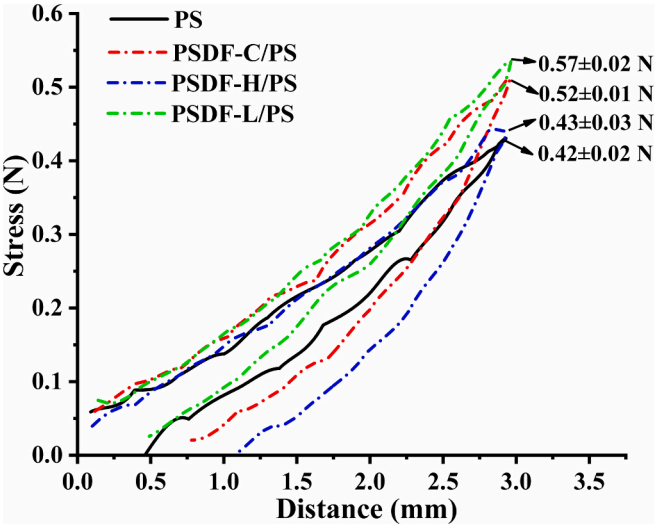

Fig. 8. Distance-stress transfer curve of PSDF/PS mixed gels.

entanglement and rearrangement of both starch molecular chains and PSDF molecular chains. PSDF-L affected the intermolecular or intramolecular interactions of starch chains, leading to a more stable mixed system. Consequently, there was a significant enhancement in both the rigidity of the gel network structure and its resistance to deformation.

4. Conclusion

This study explored the interaction mechanism between PSDF and PS during gelatinization and systematically determined the effects of PSDF on the physicochemical properties of PS gels. The results indicated that PSDFs of different Mws exerted distinct effects on starch gelatinization and the physicochemical properties of starch-based products after gelatinization. The CLSM and SAXS results revealed that PSDF could coat the surface of PS particles and loosen the lamellar structure, with PSDF-L increasing the lamellae thickness of starch. During gelatinization, PSDF-L limited starch hydration, inhibited expansion, and delayed the gelatinization process. In contrast, PSDF-H restricted starch bursting by forming a network barrier, leading to smaller fragment sizes. Furthermore, the addition of PSDF enhanced the mixed system stability and significantly increased both the degree of short-range order and the relative crystallinity of starch, imparting a more ordered network structure to the mixed gel. Additionally, while PSDF-L increased the G' and G" values of the gel, PSDF-H produced the opposite effect. Notably, the addition of PSDF-L significantly enhanced gel rigidity by 35.7 % and improved the ability of gel to resist deformation These results provide a theoretical foundation for regulating the physicochemical properties of starch-based products using dietary fiber.

Although this explained the effects of high and low Mws on starch gelatinization characteristics and gel characteristics, the study has several important associated limitations. For example, the dietary fiber subcomponents were not further analyzed. It is necessary to combine methylation and structural analysis techniques, such as nuclear magnetic resonance, to clarify the hydrogen bonds or hydrophobic interactions between fragments of different Mws and starch chains. In addition, the constant-temperature gelatinization and static cooling mode adopted in this experiment may not be capable of simulating dynamic shearing in actual industrial processes. The influence of the shear rate on the fiber–starch composite gel should be quantified through twin-screw extrusion combined with online rheological monitoring. Furthermore, the current conclusion is based on a simplified starch–fiber binary model; in real food matrices, other groups may mask or modulate the dietary fiber–starch interaction sites, which remains to be tested.

CRediT authorship contribution statement

Zhenzhen Zhang: Writing – review & editing, Writing – original draft, Methodology, Data curation, Conceptualization. **Qiannan Liu:** Visualization, Methodology, Investigation, Data curation. **Ruixuan Zhao:** Writing – review & editing, Methodology, Formal analysis, Data curation. **Jing Li:** Methodology, Data curation. **Honghai Hu:** Writing – review & editing, Funding acquisition, Data curation. **Aurore Richel:** Validation, Conceptualization.

Funding

This work was supported by the National Key Research and Development Program of China (2024YFF1105603-5); Central Public-interest Scientific Institution Basal Research Fund (S2023JBKY-04) and the earmarked fund for China Agriculture Research System (CARS-09-P27).

Declaration of competing interest

The authors declare that they have no known competing financial interests or personal relationships that could have appeared to influence

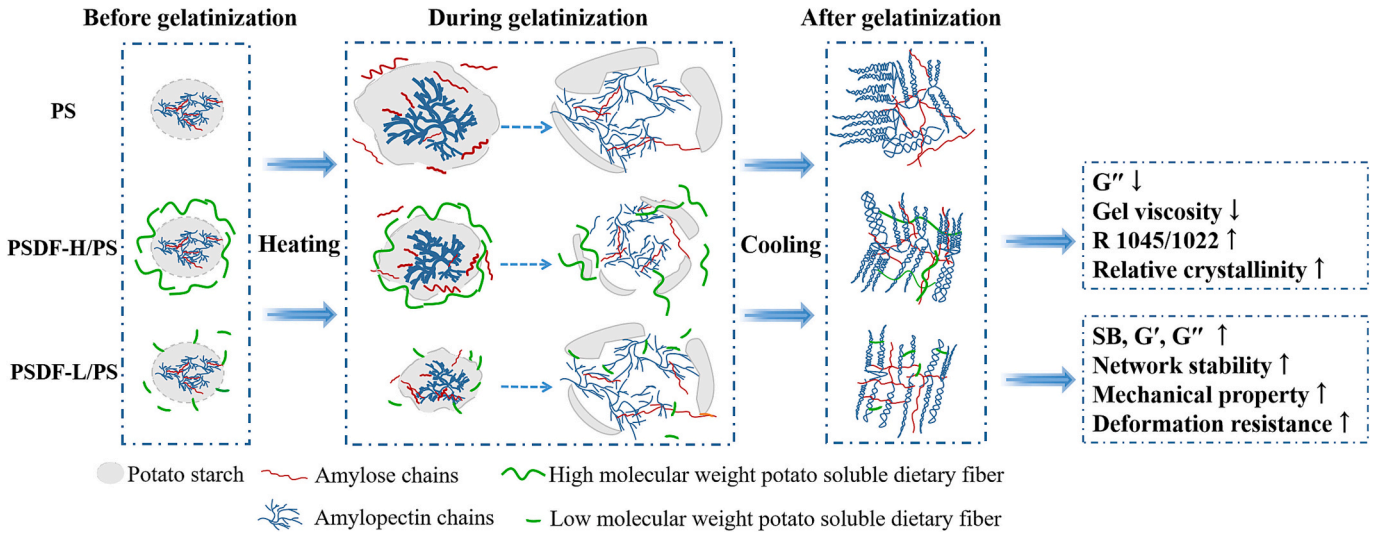

Fig. 9. Mechanism model diagram of interaction between different Mw PSDF and PS during gelatinization.

the work reported in this paper.

Appendix A. Supplementary data

Supplementary data to this article can be found online at https://doi.org/10.1016/j.ijbiomac.2025.147211.

Data availability

Data will be made available on request.

References

[1] Z. Zou, M. Li, Q. Song, B. Guo, G. Zhou, F. Xie, Regulation of retrogradation and textural properties of mung bean starch gels during storage: role of cooling rate, Carbohydr. Polym. 366 (2025) 123915, https://doi.org/10.1016/j.carbpol.2025.123915.

[2] J. Li, X. Xu, Q. Zhao, J. Zhang, P. Zhu, D. Xu, F. Wu, Effects of ratios of A- and B-type wheat starch on liangpi (a starch gel food) quality and its potential mechanism, Carbohydr. Polym. 352 (2025) 123194, https://doi.org/10.1016/j.carbpol.2024.123194.

[3] Z. Gan, M. Zhang, S. Xu, T. Li, X. Zhang, J. Wang, L. Wang, Comparison of quinoa and highland barley derived dietary fibers influence on the physicochemical properties and digestion of rice starch, Food Res. Int. 174 (Pt 1) (2023) 113549, https://doi.org/10.1016/j.foodres.2023.113549.

[4] L.A. Bello-Perez, P.C. Flores-Silva, Interaction between starch and dietary compounds: new findings and perspectives to produce functional foods, Int. Food Res. J. 172 (2023) 113182, https://doi.org/10.1016/j.foodres.2023.113182.

[5] D.N. Zhou, B. Zhang, B. Chen, H.Q. Chen, Effects of oligosaccharides on pasting, thermal and rheological properties of sweet potato starch, Food Chem. 230 (2017) 516–523, https://doi.org/10.1016/j.foodchem.2017.03.088.

[6] S. Qiu, M.P. Yadav, Y. Liu, H. Chen, E. Tatsumi, L. Yin, Effects of corn fiber gum with different molecular weights on the gelatinization behaviors of corn and wheat starch, Food Hydrocoll. 53 (2016) 180–186, https://doi.org/10.1016/j.foodhyd.2015.01.034.

[7] J.D. Torres, V. Dueik, I. Contardo, D. Carré, P. Bouchon, Relationship between microstructure formation and in vitro starch digestibility in baked gluten-starch matrices, Food Chem X 22 (2024) 101347, https://doi.org/10.1016/j.fochx.2024.101347.

[8] Y. Gong, S. Xiao, Z. Yao, H. Deng, X. Chen, T. Yang, Factors and modification techniques enhancing starch gel structure and their applications in foods: a review, Food Chem X 24 (2024) 102045, https://doi.org/10.1016/j.fochx.2024.102045.

[9] F. Yang, Q. Du, T. Miao, X. Zhang, W. Xu, D. Jia, Interaction between potato starch and Tremella fuciformis polysaccharide, Food Hydrocoll. 127 (2022) 107509, https://doi.org/10.1016/j.foodhyd.2022.107509.

[10] H. Zhang, S. Sun, L. Ai, Physical barrier effects of dietary fibers on lowering starch digestibility, Curr. Opin. Food Sci. 48 (2022) 100940, https://doi.org/10.1016/j.cofs.2022.100940.

[11] A. Matignon, G. Moulin, P. Barey, M. Desprairies, S. Mauduit, J.M. Sieffermann, C. Michon, Starch/carrageenan/milk proteins interactions studied using multiple staining and Confocal Laser Scanning Microscopy, Carbohydr. Polym. 99 (2014) 345–355, https://doi.org/10.1016/j.carbpol.2013.09.002.

[12] R. Chen, P.A. Williams, J. Shu, S. Luo, J. Chen, C. Liu, Pectin adsorption onto and penetration into starch granules and the effect on the gelatinization process and rheological properties, Food Hydrocoll. 129 (2022) 107618, https://doi.org/10.1016/j.foodhyd.2022.107618.

[13] H. Ge, F. Jin, J. Li, C. Wu, Correction to how much force is needed to stretch a coiled chain in solution? Macromolecules 42 (16) (2009) 6330, https://doi.org/10.1021/ma9005523.

[14] Y. Xu, C. Cai, K. Chandarajoti, P.-H. Hsieh, L. Li, T.Q. Pham, J. Liu, Homogeneous low-molecular-weight heparins with reversible anticoagulant activity, Nat. Chem. Biol. 10 (4) (2014) 248–250, https://doi.org/10.1038/nchembio.1459.

[15] M. Zhang, S. Xu, Z. Zuo, H. Xu, Q. Xu, T. Li, L. Wang, Modulation of rice starch physicochemical properties and digestibility: the role of highland barley non-starch polysaccharide fractions, Int. J. Biol. Macromol. 279 (Pt 4) (2024) 135206, https://doi.org/10.1016/j.ijbiomac.2024.135206.

[16] Z. Xue, Y. Chen, Y. Jia, Y. Wang, Y. Lu, H. Chen, M. Zhang, Structure, thermal and rheological properties of different soluble dietary fiber fractions from mushroom Lentinula edodes (Berk.) Pegler residues, Food Hydrocoll. 95 (2019) 10–18, https://doi.org/10.1016/j.foodhyd.2019.04.015.

[17] C. Hou, X. Zhao, M. Tian, Y. Zhou, R. Yang, Z. Gu, P. Wang, Impact of water extractable arabinoxylan with different molecular weight on the gelatinization and retrogradation behavior of wheat starch, Food Chem. 318 (2020) 126477, https://doi.org/10.1016/j.foodchem.2020.126477.

[18] A. Yuris, K.K.T. Goh, A.K. Hardacre, L. Matia-Merino, Understanding the interaction between wheat starch and Mesona chinensis polysaccharide, LWT–Food Sci. Technol. 84 (2017) 212–221, https://doi.org/10.1016/j.lwt.2017.05.066.

[19] Z. Zhang, L. Zhang, W. Liu, Q. Liu, R. Zhao, H. Hu, Potato soluble dietary fiber as a functional ingredient affects the physicochemical properties of native potato starch during freeze-thawing, Food Bioprocess Technol. 17 (7) (2023) 1997–2008, https://doi.org/10.1007/s11947-023-03252-5.

[20] C. Milanezzi, E. Silva, Role of particle size and co-extraction dynamics in the sequential recovery of phenolics, starch, and proteins from potato peel by-products, Food Res. Int. 221 (2025) 117236, https://doi.org/10.1016/j.foodres.2025.117236.

[21] J. Feng, X. Bai, Y. Li, B. Kong, M. Nuerjiang, K. Wu, Z. Li, X. Xia, Improvement on gel properties of myofibrillar protein from chicken patty with potato dietary fiber: based on the change in myofibrillar protein structure and water state, Int. J. Biol. Macromol. 230 (2023) 123228, https://doi.org/10.1016/j.ijbiomac.2023.123228.

[22] T.T.H. Nguyen, Utilization of potato peel waste in cyanobacterium Spirulina sp. cultivation for biodiesel production and subsequent hydrochar production via optimized hydrothermal carbonization process, Renew. Energy 255 (2025) 123815, https://doi.org/10.1016/j.renene.2025.123815.

[23] X. Chen, R. Gui, N. Li, Y. Wu, J. Chen, X. Wu, X. Li, Production of soluble dietary fibers and red pigments from potato pomace in submerged fermentation by Monascus purpureus, Process Biochem. 111 (2021) 159–166, https://doi.org/10.1016/j.procbio.2021.09.01.

[24] H. Goff, N. Repin, H. Fabek, D. El Khoury, M. Gidley, Dietary fibre for glycaemia control: towards a mechanistic understanding, Bioact. Carbohydr. Diet. Fibre 14 (2018) 39–53, https://doi.org/10.1016/j.bcdf.2017.07.005.

[25] J. Lattimer, M. Haub, Effects of dietary fiber and its components on metabolic health, Nutrients 2 (12) (2010) 1266–1289, https://doi.org/10.3390/nu2121266.

[26] Q. Liu, X. Duan, Y. Zhang, W. Liu, R. Zhao, Y. Wang, H. Hu, Potato cubes for the elderly with dysphagia designed through freeze-thaw impregnation technique: effect of enzymatic hydrolysis, Innovative Food Sci. Emerg. Technol. 92 (2024) 103561, https://doi.org/10.1016/j.ifset.2023.103561.

[27] H. Jian, X. Lin, W. Zhang, W. Zhang, D. Sun, Characterization of fractional precipitation behavior of galactomannan gums with ethanol and isopropanol, Food Hydrocoll. 40 (2014) 115–121, https://doi.org/10.1016/j.foodhyd.2014.02.012.

[28] R. Chang, L. Xiong, M. Li, J. Liu, Q. Sun, Fractionation of debranched starch with different molecular weights via edible alcohol precipitation, Food Hydrocoll. 83 (2018) 430–437, https://doi.org/10.1016/j.foodhyd.2018.05.033.

[29] J. Tu, B. Adhikari, M.A. Brennan, P. Cheng, W. Bai, C. Brennan, Interactions between sorghum starch and mushroom polysaccharides and their effects on starch gelatinization and digestion, Food Hydrocoll. 139 (2023) 108504, https://doi.org/10.1016/j.foodhyd.2023.108504.

[30] A. Venkatachalam, A. Balasubramaniam, P.F.C. Wilms, L. Zhang, M.A.I. Schutyser, Impact of varying macronutrient composition on the printability of pea-based inks in extrusion-based 3D food printing, Food Hydrocoll. 142 (2023) 108760, https://doi.org/10.1016/j.foodhyd.2023.108760.

[31] K. Xu, C. Chi, Z. She, X. Liu, Y. Zhang, H. Wang, H. Zhang, Understanding how starch constituent in frozen dough following freezing-thawing treatment affected quality of steamed bread, Food Chem. 366 (2022) 130614, https://doi.org/10.1016/j.foodchem.2021.130614.

[32] J. Kong, M. Shen, W. Zhang, G. Wang, J. Lin, H. Wen, J. Xie, Mesona chinensis polysaccharide regulates the gelatinization behavior of rice starch, Food Hydrocoll. 162 (2025) 110905, https://doi.org/10.1016/j.foodhyd.2024.110905.

[33] Z. Zhang, Q. Liu, L. Zhang, W. Liu, A. Richel, R. Zhao, H. Hu, Potato dietary fiber effectively inhibits structure damage and digestibility increase of potato starch gel due to freeze-thaw cycles, Int. J. Biol. Macromol. 279 (Pt 1) (2024) 135034, https://doi.org/10.1016/j.ijbiomac.2024.135034.

[34] G. Qiu, Z. Xu, J.-Y. Wu, C. Li, Z. Hu, R. Huang, X. Liu, Litchi polyphenols and carboxylated cellulose nanofiber synergistically improve the gel properties of κ-carrageenan gels: insight from rheology, morphology and interaction computational simulation, Food Hydrocoll. 166 (2025) 111292, https://doi.org/10.1016/j.foodhyd.2025.111292.

[35] J. Yang, W. Illeperuma, Z. Suo, Inelasticity increases the critical strain for the onset of creases on hydrogels, Extreme Mech. Lett. (2020) 100966, https://doi.org/10.1016/j.eml.2020.100966.

[36] Y. Luo, M. Shen, E. Li, Y. Xiao, H. Wen, Y. Ren, J. Xie, Effect of Mesona chinensis polysaccharide on pasting, rheological and structural properties of corn starches varying in amylose contents, Carbohydr. Polym. 230 (2020) 115713, https://doi.org/10.1016/j.carbpol.2019.115713.

[37] M. Zheng, Q. You, Y. Lin, F. Lan, M. Luo, H. Zeng, Y. Zhang, Effect of guar gum on the physicochemical properties and in vitro digestibility of lotus seed starch, Food Chem. 272 (2019) 286–291, https://doi.org/10.1016/j.foodchem.2018.08.029.

[38] J. Blazek, E.P. Gilbert, Application of small-angle X-ray and neutron scattering techniques to the characterisation of starch structure: a review, Carbohydr. Polym. 85 (2) (2011) 281–293, https://doi.org/10.1016/j.carbpol.2011.02.041.

[39] Z. He, L. Jiang, K. Wang, S. Chen, M. Mei, C. Sun, X. Du, Multi-scale structural heterogeneity of glutinous rice starch in different varieties: a determinant of physicochemical properties and digestibility, Int. J. Biol. Macromol. 311 (Pt 3) (2025) 143946, https://doi.org/10.1016/j.ijbiomac.2025.143946.

[40] Q. Wang, L. Li, C. Liu, X. Zheng, Heat-moisture modified blue wheat starch: physicochemical properties modulated by its multi-scale structure, Food Chem. 386 (2022) 132771, https://doi.org/10.1016/j.foodchem.2022.132771.

[41] X. Liu, S. Liu, H. Xi, J. Xu, D. Deng, G. Huang, Effects of soluble dietary fiber on the crystallinity, pasting, rheological, and morphological properties of corn resistant starch, LWT-Food Sci. Technol. 111 (2019) 632–639, https://doi.org/10.1016/j.lwt.2019.01.059.

[42] S. Qiu, M. Yadav, H. Chen, Y. Liu, E. Tatsumi, L. Yin, Effects of corn fibre gum (CFG) on the pasting and thermal behaviors of maize starch, Carbohydr. Polym. 115 (2015) 246–252, https://doi.org/10.1016/j.carbpol.2014.08.071.

[43] J. Zhuang, J. Zhu, P. Cheung, C. Li, The physical and chemical interactions between starch and dietary fiber: their impact on the physicochemical and nutritional properties of starch, Trends Food Sci. Technol. 149 (2024) 104566, https://doi.org/10.1016/j.tifs.2024.104566.

[44] X. Kong, Z. Zhu, X. Zhang, Y. Zhu, Effects of Cordyceps polysaccharides on pasting properties and in vitro starch digestibility of wheat starch, Food Hydrocoll. 102 (2020) 105604, https://doi.org/10.1016/j.foodhyd.2019.105604.
[45] H. Hu, M. Nie, M. Galluzzi, X. Yu, X. Du, Mimosa-inspired high-sensitive and multi-responsive starch actuators, Adv. Funct. Mater. 33 (45) (2023), https://doi.org/10.1002/adfm.202304634.
[46] E.C. Lee, J. Lee, H.-J. Chung, E.Y. Park, Impregnation of normal maize starch granules with ionic hydrocolloids by alkaline dry heating, Food Hydrocoll. 113 (2021) 106462, https://doi.org/10.1016/j.foodhyd.2020.106462.
[47] S. Shrestha, M.B. Sadiq, A.K. Anal, Culled banana resistant starch-soy protein isolate conjugate based emulsion enriched with astaxanthin to enhance its stability, Int. J. Biol. Macromol. 120 (Pt A) (2018) 449–459, https://doi.org/10.1016/j.ijbiomac.2018.08.066.
[48] W. Pan, X. Qi, Z. Huang, M. Shen, H. Wen, J. Xie, Effect of three polysaccharides with different charge characteristics on the properties of highland barley starch gel, Int. J. Biol. Macromol. 281 (Pt 1) (2024) 136267, https://doi.org/10.1016/j.ijbiomac.2024.136267.
[49] H. He, Y. Hao, C. Ai, K. Wang, W. Liao, J. Shen, Isolation of Dictyophora indusiata polysaccharide and its effects on the multi-structure characteristics and in vitro digestion of extruded rice starch, LWT-Food Sci. Technol. 162 (2022) 113446, https://doi.org/10.1016/j.lwt.2022.113446.
[50] J. Zheng, S. Huang, R. Zhao, N. Wang, J. Kan, F. Zhang, Effect of four viscous soluble dietary fibers on the physicochemical, structural properties, and in vitro digestibility of rice starch: a comparison study, Food Chem. 362 (2021) 130181, https://doi.org/10.1016/j.foodchem.2021.130181.
[51] Y. Feng, T. Mu, M. Zhang, M. Ma, Effects of different polysaccharides and proteins on dough rheological properties, texture, structure and in vitro starch digestibility of wet sweet potato vermicelli, Int. J. Biol. Macromol. 148 (2020) 1–10, https://doi.org/10.1016/j.ijbiomac.2019.12.225.
[52] Y. Lin, Y.H. Roos, S. Miao, Transglutaminase crosslinked fish gelatin emulsion gels: structure, rheology behaviors, and delivery functionality, Food Hydrocoll. 162 (2025) 111001, https://doi.org/10.1016/j.foodhyd.2024.111001.
[53] M. Anvari, M. Tabarsa, H.S. Joyner, Large amplitude oscillatory shear behavior and tribological properties of gum extracted from Alyssum homolocarpum seed, Food Hydrocoll. 77 (2018) 669–676, https://doi.org/10.1016/j.foodhyd.2017.11.008.
[54] H. Jung, T.M. Oyinloye, W.B. Yoon, Evaluating the mechanical response of agarose-xanthan mixture gels using tensile testing, numerical simulation, and a Large Amplitude Oscillatory Shear (LAOS) approach, Foods 11 (24) (2022) 4042, https://doi.org/10.3390/foods11244042.
[55] Q. Li, M. Xu, J. Xie, E. Su, Z. Wan, L.M.C. Sagis, X. Yang, Large amplitude oscillatory shear (LAOS) for nonlinear rheological behavior of heterogeneous emulsion gels made from natural supramolecular gelators, Food Res. J. 140 (2021) 110076, https://doi.org/10.1016/j.foodres.2020.110076.
[56] X. Yin, Y. Zheng, X. Kong, S. Cao, S. Chen, D. Liu, J. Tian, RG- i pectin affects the physicochemical properties and digestibility of potato starch, Food Hydrocoll. 117 (2021) 106687, https://doi.org/10.1016/j.foodhyd.2021.106687.
[57] H. He, C. Chi, F. Xie, X. Li, Y. Liang, L. Chen, Improving the in vitro digestibility of rice starch by thermomechanically assisted complexation with guar gum, Food Hydrocoll. 102 (2020) 105637, https://doi.org/10.1016/j.foodhyd.2019.105637.
[58] A. Pourfarzad, A. Yousefi, K. Ako, Steady/dynamic rheological characterization and FTIR study on wheat starch-sage seed gum blends, Food Hydrocoll. 111 (2021) 106380, https://doi.org/10.1016/j.foodhyd.2020.106380.
[59] J. Kong, J. Song, H. Wen, Q. Yu, Y. Chen, J. Xie, A comparative study on the gel and structural characteristics of starch from three rice varieties when combined with Mesona chinensis polysaccharides, Int. J. Biol. Macromol. 269 (Pt 1) (2024) 132114, https://doi.org/10.1016/j.ijbiomac.2024.132114.
[60] F. Warren, M. Gidley, B. Flanagan, Infrared spectroscopy as a tool to characterise starch ordered structure-a joint FTIR-ATR, NMR, XRD and DSC study, Carbohydr. Polym. 139 (2016) 35–42, https://doi.org/10.1016/j.carbpol.2015.11.066.